ELSEVIER

Journal of Nuclear Materials 298 (2001) 211–224

journal of nuclear materials

www.elsevier.com/locate/jnucmat

Microstructural characterization of irradiation-induced Cu-enriched clusters in reactor pressure vessel steels

R.G. Carter [a,*], N. Soneda [b], K. Dohi [b], J.M. Hyde [c], C.A. English [c], W.L. Server [d]

[a] *EPRI, 1300 W.T. Harris Boulevard, Charlotte, NC 28262, USA*
[b] *Central Research Institute of Electric Power Industry, 2-11-1 Iwado Kita, Komae-shi, Tokyo, 201-8511, Japan*
[c] *AEA Technology, B220, Harwell, Didcot, Oxon OX11 0RA, UK*
[d] *ATI Consulting, PO Box 5769, Pinehurst, NC 28374, USA*

Received 24 March 2000; accepted 20 July 2001

Abstract

The effect of irradiation on microstructure of four irradiated reactor pressure vessel steels (a low copper A533B-1 plate, a low copper A508-3 forging, a high copper Linde 80 flux weld and a high copper Linde 1092 flux weld) was determined by using complementary microstructural techniques such as optical position-sensitive atom probe (OPoSAP), field emission gun scanning transmission electron microscopy (FEGSTEM) and small angle neutron scattering (SANS). In the low copper steels, irradiation resulted in small shifts in transition temperature and small changes in hardness increments. The microstructural analyzes showed that this response was dominated by matrix damage. In contrast, both copper-enriched clusters and matrix damage formed in the high copper welds. This information was then used as input to the Russell–Brown model to predict the change in hardness resulting from copper-enriched clusters. The calculated hardness increments were found to be consistent with the experimental data. © 2001 Published by Elsevier Science B.V.

PACS: 61.80.Hg; 61.82.Bg; 81.40.Cd; 81.70.Bt

1. Introduction

There has been increased emphasis in underpinning existing trend curves by furthering the understanding of the controlling mechanisms that cause reactor pressure vessel (RPV) embrittlement. This involves detailed characterization of the irradiation-induced microstructual changes and their dependence on material and irradiation parameters. Three basic micromechanisms of irradiation embrittlement have been identified [1,2]:

1. Irradiation enhanced precipitation of copper which leads to the formation of precipitates or clusters enriched in Cu, Mn, Ni and Si. The distinction between precipitates and clusters is that clusters are less well defined than precipitates and also contain iron.
2. Matrix damage due to radiation produced point defect clusters and dislocation loops.
3. Irradiation-induced/enhanced grain boundary segregation of embrittling elements such as phosphorus.

The first two mechanisms serve to harden the material and increase the yield strength (σ_y), while the third mechanism causes a drop in the fracture strength (σ_F). The effect of irradiation in causing hardening or a change in σ_F is to cause a change in the transition temperature.

The objectives of this paper are to fully characterize the irradiation-induced copper precipitation in a range of commercial steels and to correlate the results with measured mechanical property changes and understand the results based on known models and mechanisms of embrittlement. RPV base metals (low copper A533B-1 plate and low copper A508-3 forging)

* Corresponding author. Tel.: +1-704 547 6019; fax: +1-704 547 6035.
E-mail address: bcarter@epri.com (R.G. Carter).

0022-3115/01/$ - see front matter © 2001 Published by Elsevier Science B.V.
PII: S0022-3115(01)00659-6

and welds (high copper Linde 80 flux weld and high copper Linde 1092 flux weld) were chosen for this study to ensure that the results are applicable to operating reactors materials. Microstructural techniques, comprised of field emission gun scanning transmission electron microscopy (FEGSTEM), optical position-sensitive atom probe (OPoSAP) and small angle neutron scattering (SANS), were used to study copper precipitation.

An overview of the experimental program is presented in Section 2, with details of the materials and irradiation conditions (Section 2.1) and a brief description of the microstructural techniques employed and their capabilities (Section 2.2). The results are presented in Section 3. The mechanical property data is presented first, followed by the microstructural data obtained from each material. Section 4 details the main trends and links the microstructural data to the observed mechanical properties. Conclusions are presented in Section 5.

2. Experimental details

2.1. Materials and irradiation conditions

The materials and the irradiation conditions investigated are listed in Tables 1 and 2. Stress relief annealing was performed on two weld metals, BW2 and CE1, while no stress relief annealing was performed on two base metals, EP2 and EF2, designated as NSR in Table 2. The plate material, EP2, is essentially the equivalent of a low copper plate material, identified as specimens 1B, and additional irradiated shift data are available for plate 1B at very high fluence levels from the Japan Materials Test Reactor (JMTR) irradiation program [3]. The EF2 material is a forging material with low copper similar to the EP2 plate material.

2.2. Microstructural techniques

2.2.1. Characterization of copper precipitation

A methodology to determine reliable experimental data on copper precipitation is presented. The important parameters in characterizing copper precipitation are matrix copper content and the composition, size and number density of copper-enriched precipitates/clusters. There are very reliable experimental techniques such as FEGSTEM [4], OPoSAP [5] and SANS [6]. However, no single technique can provide a full characterization, and therefore, iterative use of these techniques is required to determine a description of the microstructure which is consistent with all of the microstructural information. The techniques employed in this study are discussed below and summarized in Table 3.

2.2.1.1. FEGSTEM. A perchloric-based electrolyte was used in a Tenupol™ twin jet polisher to prepare thin foils specimens for FEGSTEM analysis. These foils were immediately dipped in a chromic/acetic acid mix to remove any traces of copper deposited during electropolishing. Typically the observed areas of these foils are 50–100 nm thick.

FEGSTEM was used in two modes: 'spot' mode and 'small area scan' mode. When used in 'spot' mode, the electron beam is focused on a region that is <2 nm in diameter and thus can be used to study features as small as ≈1.5–2 nm (the resolution limit). It should be noted that if the electron beam is focused on a feature of diameter 2 nm, the resultant energy spectrum results from both the feature and matrix since the electron beam passes through the foil which is primarily occupied by the matrix. This means that an analysis of the spectrum provides the mean composition within the analyzed volume. The difference between data taken with the electron beam focused on a small feature and focused on neighboring matrix shows which elements are enriched

Table 1
Bulk chemical composition of materials (wt%)

Material ID	Type	Cu	Ni	P	S	C	Cr	Mo	Mn	Si
BW-2	Linde 80 flux weld	0.30	0.58	0.017	0.012	0.08	0.10	0.39	1.63	0.61
CE-1	Linde 1092 flux weld	0.21	1.00	0.014	0.009	0.13	0.05	0.54	1.23	0.21
EP2	A533B-1 plate	0.06	0.59	0.008	0.007	0.19	–	0.49	1.42	0.20
EF2	A508-3 forging	0.04	0.75	0.008	0.007	0.19	0.09	0.49	1.40	0.24

Table 2
Irradiation conditions and materials

Capsule ID	Flux $E > 1$ MeV (n/cm^2 s)	Fluence $E > 1$ MeV (n/cm^2)	Temp (°C)	Linde 80 flux weld	Linde 1092 flux weld	A-533B-1	A-508-3
				BW2	CE1	EP2 NSR	EF2 NSR
MTR1	5×10^{12}	1.13×10^{18}	288	–	–	X	X
MTR3	5×10^{12}	2.74×10^{19}	288	X	X	X	–

Table 3
Summary of microstructural techniques employed

Technique	Information on matrix damage?	Information on irradiation-induced clusters?	Information on non-hardening embrittlement?
FEGSTEM	No (although dislocation loops may provide contrast)	Provides approximate concentrations of alloying elements (excluding Fe)	Yes from analysis of grain boundaries. Profile across boundary provides estimate of coverage
OPoSAP	No	Direct analysis of clusters – size and composition	Limited since the probability of analyzing a grain boundary is low
SANS	Limited – interpretation difficult	Cluster size. *A*-ratio is linked to composition. Number density if cluster composition is known	No

in the feature and can be used to estimate the ratio of elements in the feature excluding iron. The presence of unresolvable features can be determined by taking a series of spot measurements. If compositions measured in the spot mode distribute in a wide range, then that means a non-uniform distribution of copper.

If the electron beam is not so highly focused, small area measurements can yield the copper content between easily identifiable features to ± 0.05 wt% or better. However, the measurements will also average over unresolvable features ($<\sim 1.5$ nm) if they exist. Therefore the FEGSTEM yields the following information.

- A direct measurement of matrix copper if no precipitation has occurred, or if the precipitates/clusters are all resolvable by TEM techniques.
- If a low number density of unresolvable precipitates is found, then the minimum observed compositions determined from spot values may be used to estimate the matrix copper levels.
- The ratio of elements excluding iron in the precipitates.

2.2.1.2. OPoSAP. Data from an OPoSAP analysis can be used to reconstruct the atomic-scale microstructure of a material in 3D. Therefore, it enables the direct interpretation of cluster morphology and composition of nanometer-scale irradiation-induced clusters. Needle shaped specimens with an end radius of ~ 50 nm are produced by electropolishing. During analysis, a small volume is analyzed (typically $10 \times 10 \times 100$ nm^3). Therefore the technique is limited by poor statistics since typically only a few clusters are analyzed per specimen. The OPoSAP yields an accurate measurement of matrix copper within a small volume and composition, size and morphology of any precipitates/clusters within the analyzed volume.

From the above discussion it can be seen that the combination of the FEGSTEM (having good statistics) and atom probe microanalysis (having high accuracy) can be used to characterize the matrix level of copper and the composition of the precipitates/clusters. However, neither can be used to provide an accurate assessment of the number density of particles present.

2.2.1.3. SANS. Only one technique, SANS, can provide data on the size distribution of irradiation-induced precipitates/clusters. The experimental arrangement dictates the minimum size of inhomogeneity that can be detected. The best instruments can detect precipitates/clusters as small as 1 nm in size in samples that are typically $\sim 10 \times 10 \times 2$ mm^3 in size.

Analysis involves measuring the differential scattering cross-section, $\mathrm{d}\sigma/\mathrm{d}\Omega$, of the material of interest in zero magnetic field and with the scattering vector both parallel and perpendicular to an applied magnetic field. Measurements are taken for the material in both irradiated and unirradiated conditions and then normalized to determine the absolute differential scattering cross-sections. Subtraction yields the irradiation-induced component which can then be analyzed.

Information on the chemical composition of the irradiation-induced precipitates/clusters is obtained via the *A*-ratio:

$$A\text{-ratio} = \frac{(\mathrm{d}\sigma/\mathrm{d}\Omega)_{\perp}}{(\mathrm{d}\sigma/\mathrm{d}\Omega)_{\parallel}} = \frac{N+M}{N}, \tag{1}$$

where N and M are the nuclear and magnetic components of the differential cross-section arising from the respective contrast between the precipitates/clusters and matrix.

The *A*-ratio is sensitive to chemical, structural and magnetic differences between the precipitates/clusters and matrix, and should be consistent with precipitate compositional information obtained from FEGSTEM or OPoSAP microanalyses.

Once the precipitate/cluster composition has been identified, the SANS data can be further interpreted in terms of volume fraction and precipitate or cluster number density. If the precipitates/clusters contain iron in a magnetic state, then the contrast between the precipitate/cluster and matrix will decrease. As the contrast decreases, the calculated volume fraction (and hence number density) of precipitates/clusters must increase to account for the observed scattering intensity. Consequently, the 'precipitate' number density is strongly

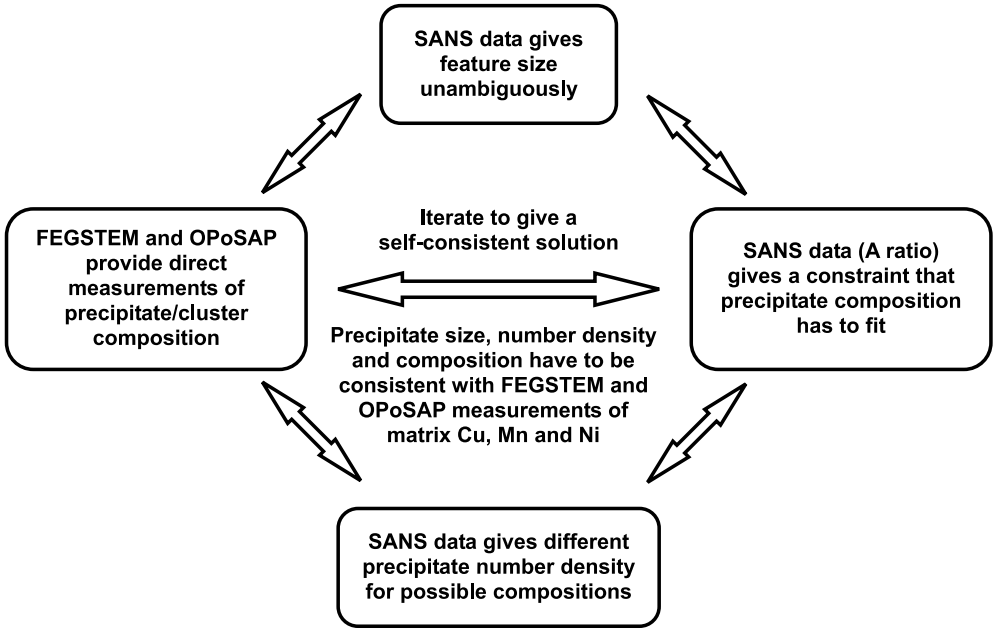

Fig. 1. Methodology for interpretation of microstructural data.

dependent on the quantity of magnetic iron assumed to be associated with the 'precipitates'.

2.2.1.4. Combining the FEGSTEM, OPoSAP and SANS data. The methodology for obtaining a self-consistent solution detailing the fine scale precipitation of copper is shown schematically in Fig. 1. Once a consistent set of results has been obtained for materials containing irradiation-induced clusters, the data can be used in the Russell–Brown model for precipitation hardening [7] and an estimate can be made for the contribution to the increased hardness caused by the irradiation-induced precipitation of copper-enriched precipitates/clusters.

2.2.2. Characterization of grain boundary segregation

The FEGSTEM can be used to measure the segregation of elements such as phosphorus to grain boundaries. Measurements on the boundary, ± 2, ± 5 and ± 10 nm away from the boundary are used to generate a composition profile. The height and width of the profile can then be used to calculate the monolayer coverage, that is the fraction of a monolayer that would need to be covered to generate the observed profile [8].

3. Results

3.1. Mechanical properties

The emphasis has been on determining Charpy V-notch properties and comparing the results from test reactor experiments with results from commercial surveillance capsules and/or other test reactors. These comparisons are shown in Figs. 2–4 [3,9–14]. Table 4 summarizes the results from the test reactor irradiations.

The base metals (EP2 and EF2) show small shifts in transition temperature even for high fluence levels (Fig. 2); scatter in the data becomes more of a problem when evaluating small shifts. The Japanese prediction equations, JEAC 4201 [15] for EP2 over-predict the low fluence test reactor results from this study, but under predict the high fluence results for the JMTR experiments. The small shift values are, however, within typical scatter for Charpy V-notch tests.

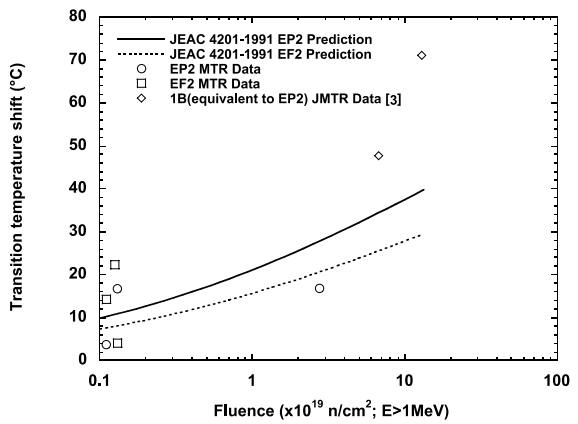

Fig. 2. Comparison of Charpy shift results for EP2 and EF2 base metals with Japanese shift prediction.

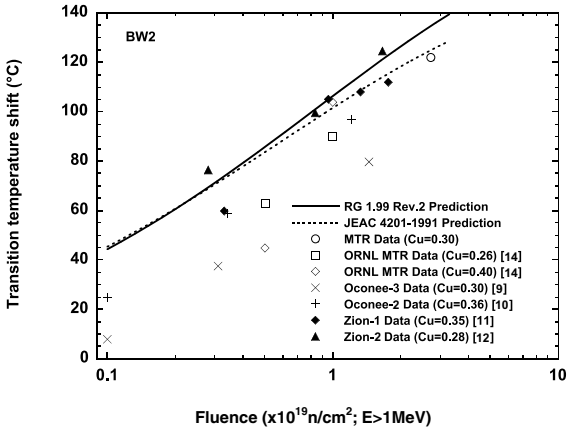

Fig. 3. Comparison of Charpy shift results for BW2 weld metal with Reg. Guide 1.99 Rev. 2 prediction (0.3% Cu, 0.58% Ni).

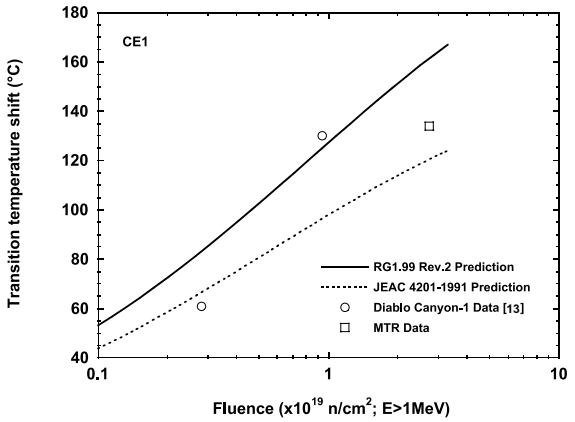

Fig. 4. Comparison of Charpy shift results for CE1 weld metal with Reg. Guide 1.99 Rev. 2 prediction (0.21% Cu, 1.0% Ni).

The Linde 1092 weld, CE1, with lower bulk copper (Fig. 4) shows larger Charpy shift than the Linde 80 weld, BW2 (Fig. 3), which has a much higher bulk copper content. In addition the test reactor results for both welds are consistent with the power reactor results for the same weld. The BW2 weld has a variety of bulk copper/nickel chemistries depending upon the exact weldment tested. Both welds exhibit behavior less than that predicted by USNRC Regulatory Guide 1.99, Revision 2 [16].

3.2. Microstructural evaluation

3.2.1. EP2 (SA533B-1 base metal, low copper)

EP2 was irradiated in two different capsules (see Table 2). The sample irradiated in MTR1 received a fluence of 1.13×10^{18} n/cm^2 ($E > 1$ MeV) whereas samples in MTR3 received a fluence of 2.74×10^{19} n/cm^2 ($E > 1$ MeV). The flux of 5×10^{12} n/cm^2 s ($E > 1$ MeV) was the same in both capsules. Analysis of the unirradiated material showed that the microstructure consists of mixed ferrite-tempered martensite and bainite with a grain size of 20–30 μm. Discrete aligned inclusions between 2 and 34 μm were observed. Carbides were found on both grain and lath boundaries and other larger precipitates (~100 nm) were Mn-rich, Mo-rich or Mn/Si-rich. Irradiation had no detectable effect on these precipitates.

The FEGSTEM spot measurements were narrow and showed no substantial evidence for uneven copper distribution following either irradiation although the distribution was slightly greater in the higher dose material (Figs. 5(a), (b)). In both irradiation conditions, the best estimate of the matrix copper was only 0.01% lower than the mean small area measurement indicating either that no irradiation-induced copper-enriched clusters had formed or that their number density was very low. Furthermore, no small features exhibiting black white contrast, typical of copper containing irradiation-induced clusters, could be identified. Analysis of four prior austenite grain boundaries in each material showed enhanced levels of phosphorus at the boundaries (~6% monolayer coverage). However no substantial differences were observed between boundaries in the two irradiated materials suggesting that the radiation enhanced segregation is not significant.

OPoSAP microanalyzes were performed on both the low dose and high dose plate steel. Atom maps were generated which showed that the 3D distributions of copper atoms within the analyzed volume were random and no evidence for clustering was found. In the low dose material, the mean copper content was 0.10 ± 0.01

Table 4
Mechanical property results for MTR-1 and MTR-3 irradiations

Material	Capsule	Fluence ($\times 10^{19}$ n/cm^2)	T_{41J} [initial] (°C)	ΔT_{41J} (°C)	USE [initial] (J)	ΔUSE (% decrease)	H_v [initial] (20 kg @ RT)	ΔH_v (20 kg @ RT)
EF2	MTR-1	0.113	−72	14	195	5	206	14
EP2	MTR-1	0.113	−41	4	152	7	198	12
EP2	MTR-3	2.74	−41	17	152	10	198	23
CE1	MTR-3	2.74	−41	134	147	44	208	60
BW2	MTR-3	2.74	−2	122	88	34	193	41

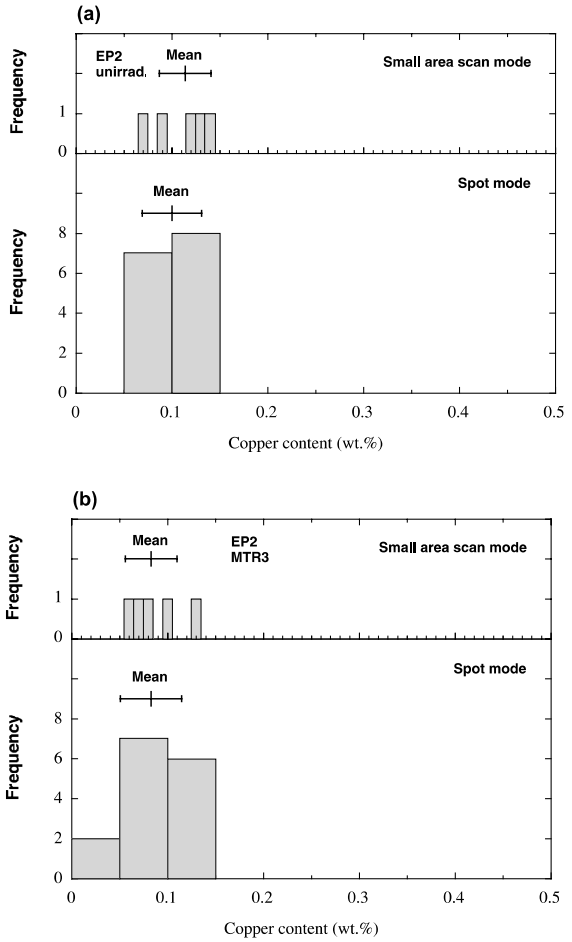

Fig. 5. FEGSTEM spot distributions for EP2 (a) unirradiated and (b) MTR-3 irradiated.

wt%. In the high dose material the mean copper concentration within the analysis volume was 0.11 ± 0.02 wt%.

SANS analysis was performed on the plate material in the unirradiated form, after a low dose in MTR1 and after a high dose in MTR3. Analysis of the irradiation-induced component showed that a small number of precipitate features with a mean size of $\approx$1.5 nm had formed during irradiation. The *A*-ratio from irradiation-induced features in the lower dose material was 1.5 whereas in the higher dose material it was 2.3. Further interpretation to determine the number density of clusters is difficult without knowing the cluster compositions in advance. Therefore a range of different cluster compositions, each being consistent with the observed *A*-ratio, was tried. For each, the cluster number density and reduction in matrix copper was calculated. The results given in Tables 5 and 6 show the following.

- An increase in the number density of features with dose.
- The number density of features is extremely low even after a fluence of 2.73×10^{19} n/cm^2 ($E > 1$ MeV).
- If the features do contain copper, then the associated reduction in matrix copper is too low to measure in the FEGSTEM or OPoSAP.

The data from each technique is consistent. The sensitivity of the SANS has demonstrated the presence of a low number density of very small features in both irradiation conditions of EP2. The number density is too low to have a realistic chance of being observed in an OPoSAP analysis and the features are too small to be resolved in the FEGSTEM. It is not possible to identify the features. They may be clusters containing Cu, Mn, and Ni or the features might simply result from matrix damage in the material.

3.2.2. EF2 (SA508-3 base metal, low copper)

Grain boundaries in EF2 following irradiation in MTR1 were enriched in phosphorus (up to 4% monolayer coverage). No data were obtained from the unirradiated forging and therefore it is not possible to determine the rate of irradiation-induced segregation. No black/white contrast features corresponding to irradiation-induced copper containing clusters were observed in the matrix of the irradiated material. The homogeneous distribution of copper was confirmed by the consistency (similar magnitude and range) between the small area (0.09 ± 0.03 wt% Cu) and spot (0.08 ± 0.02 wt% Cu) measurements.

A random area atom probe microanalysis was performed using the OPoSAP. The field ion image was very dark which is indicative of a high carbon concentration. Peaks at 6, 12, 18, 24 and 36 were observed in the mass spectrum confirming the presence of carbon. The

Table 5
Possible precipitate compositions consistent with an *A*-ratio of 1.5 (as observed from features in EP2 irradiated in MTR1)

Cu	Mn	Ni	Precipitate volume fraction	Precipitate number density (10^{23} m^{-3})	Cu in precipitates (at.%)
100 + voids	–	–	0.000002	0.01	0.0002
70.2	24.2	5.6	0.000085	0.48	0.006
46.4	53.6	–	0.000046	0.26	0.002
36.8	55.3	7.9	0.000046	0.26	0.002

Mean feature diameter 1.5 nm. Compositions in at.%.

Table 6
Possible precipitate compositions consistent with an A-ratio of 2.3 (as observed from features in EP2 irradiated in MTR3)

Cu	Mn	Ni	Precipitate volume fraction	Precipitate number density (10^{23} m^{-3})	Cu in precipitates (at.%)
100 + voids	–	–	0.000031	0.22	0.003
70.2	24.2	5.6	0.00020	1.4	0.01
72.2	27.8	–	0.00018	1.3	0.01
56.8	32.9	10.3	0.00017	1.2	0.01
47	33.7	19.3	0.00018	1.2	0.008

Mean feature diameter 1.4 nm. Compositions in at.%.

composition analysis indicated that the region analyzed was cementite (Fe_3C) with some iron substituted by manganese (10.7 wt%). The copper found during the analysis was homogeneously distributed at a concentration of 0.07 ± 0.01 wt%.

SANS experiments were performed on both the unirradiated and irradiated samples of the forging EF2. The difference in the differential scattering cross-sections was analyzed to determine the effect of irradiation in MTR1 on the distribution of small precipitate features. The analysis showed that a small number of precipitate features $\approx$1.5 nm in diameter formed with an A-ratio of 2 during irradiation. As with EP2, no data were available detailing the composition of the features. Table 7 shows that if it is assumed that the features contain Cu, Mn and Ni, their number density is extremely low ($\sim 3 \times 10^{22}$ m^{-3}) which would explain why no features were observed in the OPoSAP or FEGSTEM.

3.2.3. BW2 (Linde 80 flux weld, high copper)

Optical microscopy showed that BW2 has a dendritic microstructure consisting of bainite with carbides at grain boundaries. Larger inclusions were characterized by X-ray microanalysis in a scanning electron microscope (SEM) and found to be mostly manganese silicates with some sulfur and aluminum present.

FEGSTEM microanalysis of the unirradiated material showed that the matrix copper was 0.20 ± 0.02 wt% whereas the nominal bulk copper content was 0.30 wt%. However, there was no evidence for small copper containing clusters. Conventional atom probe confirmed the absence of small precipitates and that the matrix copper content was 0.20 ± 0.02 wt%. It was therefore concluded that either the low copper content must reflect weld to weld variations, which would be consistent with the known copper variability in the 72105 weldments [17], or that copper had precipitated during the post-weld heat-treatment.

Following irradiation in MTR3, the distribution of FEGSTEM spot analyzes was significantly broader than observed for the unirradiated material which demonstrates the presence of small copper containing irradiation-induced clusters (Figs. 6(a), (b)). The best estimate of matrix copper was 0.10 ± 0.02 wt% and therefore $\approx$0.1 wt% copper is associated with the nanometer-scale particles.

An analysis of features exhibiting black/white contrast showed that these 2 nm regions were enriched in Cu, Ni, Mn, Si and P. A comparison of the spectra obtained with the electron beam focused on the contrast feature with a neighboring region, and making the assumption that the cluster did not contain any iron, showed that the mean cluster composition is $\sim$40 wt% Cu, $\sim$24 wt% Ni, $\sim$14 wt% Mn, $\sim$11 wt% Si, $\sim$5 wt% Mo and sim4 wt% P. These compositions should be treated with caution because they result from the analysis of a small difference between spectra and therefore the errors may be considerable.

Concentration profiles were taken through two grain boundaries in the unirradiated BW2 weld and across four boundaries in the irradiated material. As a result of irradiation, three of the four grain boundaries examined showed an increase in phosphorus by 8% monolayer coverage on average.

Table 7
Possible precipitate compositions consistent with an A-ratio of 2 (as observed from features in EF2 irradiated in MTR1)

Cu	Mn	Ni	Precipitate volume fraction	Precipitate number density (10^{23} m^{-3})	Cu in precipitates (at.%)
100 + voids	–	–	0.000006	0.03	0.0006
70.2	24.2	5.6	0.000057	0.32	0.004
66.9	33.1	–	0.000046	0.26	0.003
56.7	36.0	7.3	0.000045	0.26	0.003
47	37.8	15.2	0.000045	0.26	0.002

Mean feature diameter 1.5 nm. Compositions in at.%.

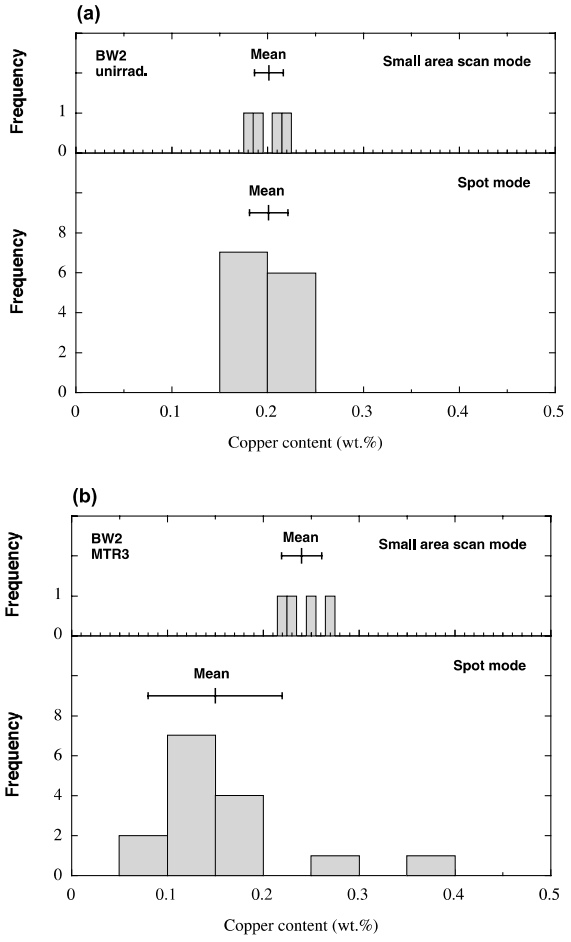

Fig. 6. Comparison of spot and small area measurements in weld BW2 (a) unirradiated and (b) MTR-3 irradiated.

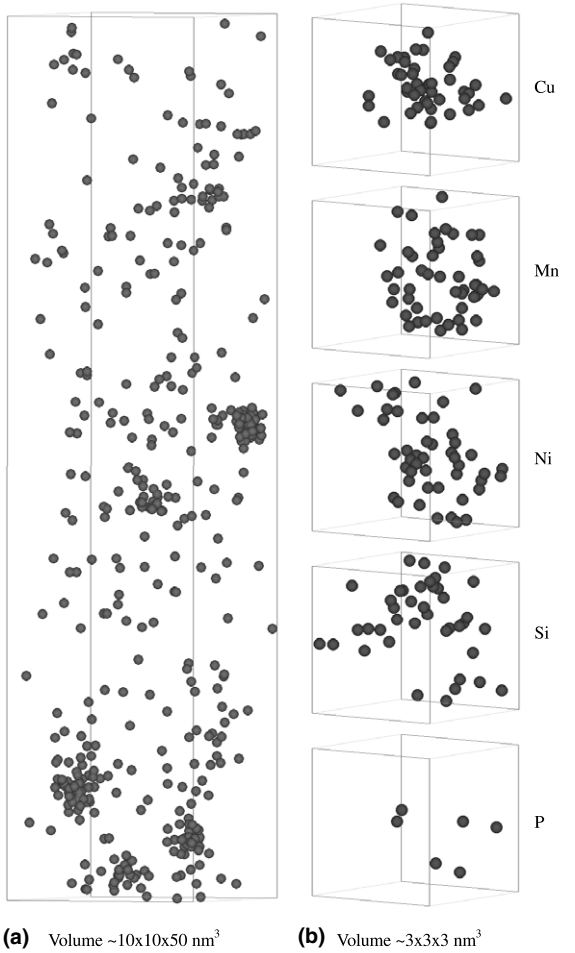

Fig. 7. OPoSAP analysis of BW2 irradiated in MTR3 (a) atom map shows the spatial distribution of copper atoms and (b) the distribution of atoms within a cluster.

The OPoSAP analysis confirmed the presence of irradiation-induced clusters each 1.5–2 nm in diameter (Fig. 7). The magnified view of one cluster (Fig. 7(b)) shows that it contains Cu, Mn, Ni and Si and that they are dilute – the majority element is iron which is consistent with previous atom probe studies of irradiation-induced precipitates [18,19]. A compositional analysis showed that the mean composition of the three best defined clusters was 55–70 wt% Fe, 20–33 wt% Cu, 2–5 wt% Mn, 2–7% wt% Si and 5–11 wt% Ni. Interestingly, the phosphorus atoms were found to be concentrated near to, but not within, the copper clusters. The number of clusters observed within the analyzed volume was also used to estimate the cluster density ($\sim 1 \times 10^{24}$ m^{-3}) and the matrix copper (0.12 wt%) was computed from those regions within the analyzed volume that did not contain clusters.

SANS analysis of the difference in the scattering vectors between the irradiated and unirradiated samples showed that during irradiation, precipitates formed with a distribution of sizes centered on 2.1 nm with a mean A-ratio of 3.1. Further interpretation of the data was performed using the compositions determined by FEGSTEM and OPoSAP microanalyzes. Two specific scenarios were considered:

- Assume the clusters do not contain iron. In this case the clusters are considered to be non-magnetic.
- Assume the clusters do contain iron as indicated by several atom probe studies in which the magnetic state of the clusters is not known.

Table 8 summarizes some of the possible precipitate compositions consistent with an A-ratio of 3.1.

The second scenario, assuming that the iron in the clusters has a magnetic moment of 0.7, provided a self-consistent picture (cluster size, composition, number density, matrix copper depletion) and demonstrates how all the data from each technique (FEGSTEM, OPoSAP and SANS) can be unified.

Table 8
Possible precipitate compositions consistent with an *A*-ratio of 3.1 (as observed from features in BW2 irradiated in MTR3)

Fe	Cu	Mn	Ni	Si	Precipitate number density (10^{23} m^{-3})	Cu in precipitates (at.%)
–	70.2	24.2	5.6	–	2.9	0.10
–	80.8	19.2	–	–	3.1	0.12
–	57.2	24.3	18.5	–	3.1	0.08
–	47.2	27.2	25.6	–	3.1	0.07
59 (magnetic)	26.5	3.5	8	3	16	0.21
59 (non-magnetic)	26.5	3.5	8	3	3.1	0.04
59 (0.7 normal magnetic moment)	26.5	3.5	8	3	7.4	0.09

Mean feature diameter 2.1 nm. Compositions in at.%.

3.2.4. CE1 (Linde 1092 flux weld, high copper)

The microstructure of weld CE1 is typical of upper bainite. Large inclusions contained Mn–Si–S–Al, although it was not possible to differentiate between sulfur and molybdenum because the S_k and Mo_L X-ray peaks obtained from X-ray microanalysis in a SEM are coincident. TEM examination showed the presence of large M_XC precipitates on grain boundaries together with some larger spherical precipitates and a small number of irregularly shaped inclusions.

FEGSTEM matrix measurements in the unirradiated alloy showed that both the spot and small area copper concentration scans gave identical results ~0.2 wt%. This value is within experimental error of the quoted bulk composition. There was no evidence for nanometer-scale copper particles. A wider distribution of spot mode measurements was obtained from the irradiated alloy indicating the non-uniform distribution of copper (Figs. 8(a), (b)). Furthermore the mean spot measurement (0.13 ± 0.03 wt% Cu) was lower than the mean of the small area measurements (0.17 ± 0.02 wt% Cu). The best estimate of the matrix copper content is 0.10 ± 0.02 wt%. The results strongly indicate the presence of nanometer-scale copper-enriched particles. FEGSTEM analysis of grain boundaries in the unirradiated material was also performed. One boundary showed more than 4% coverage phosphorus. After irradiation in MTR3, three out of four boundaries showed increased phosphorus levels of up to 7% coverage.

Conventional atom probe microanalysis of the unirradiated material showed that the copper was uniformly distributed throughout the analysis volume. The mean concentration was 0.21 ± 0.03 wt% Cu, consistent with the quoted bulk value (0.21 wt%). An OPoSAP analysis of the alloy irradiated in MTR3 showed that the mean copper content was 0.19 ± 0.02 wt% but that the copper was not distributed uniformly. An analysis of a <2 nm cluster showed that it contained ~15 wt% Cu, ~10 wt% Mn, ~5 wt% Ni, ~2 wt% Si and ~68 wt% Fe. The matrix copper content of the alloy was estimated to be 0.13 ± 0.02 wt% Cu by calculating the mean copper content in the analysis volume excluding the copper rich cluster. The atom probe analysis demonstrates the presence of copper clusters after irradiation and that the matrix copper concentration is reduced by ~0.08 wt% during irradiation.

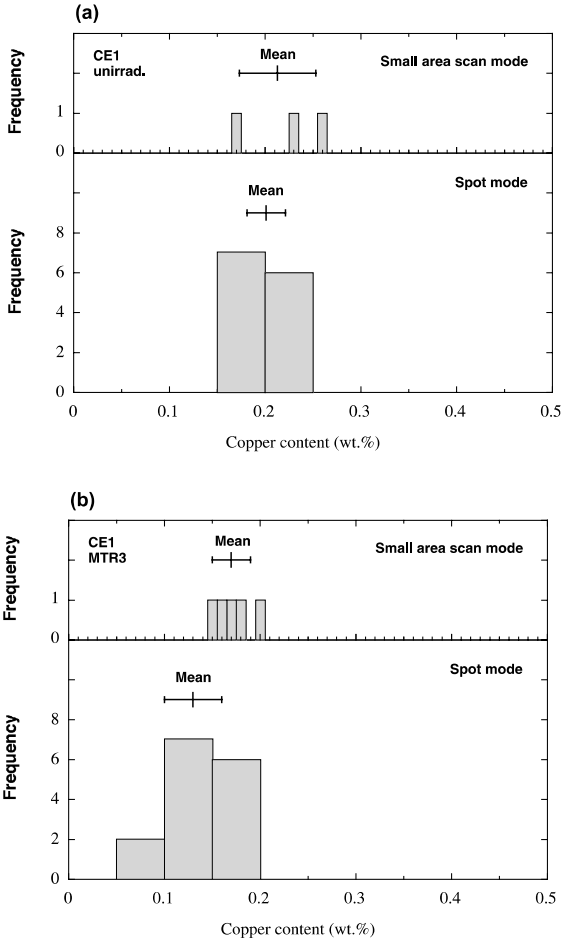

Fig. 8. Comparison of spot and small area measurements in weld CE1 (a) unirradiated and (b) MTR-3 irradiated.

SANS experiments were performed on both the unirradiated and irradiated alloys. The analysis of the irradiation-induced differential scattering cross-sections

Table 9
Possible precipitate compositions consistent with an A-ratio of 2.7 (as observed from features in CE1 irradiated in MTR3)

Fe	Cu	Mn	Ni	Si	Precipitate number density (10^{23} m^{-3})	Cu in precipitates (at.%)
–	70.2	24.2	5.6	–	4.3	0.15
–	77	23	–	–	4.3	0.16
–	57	15.4	27.6	–	4.3	0.12
–	47.2	27.3	25.5	–	4.3	0.10
68 (magnetic)	15	10	5	2	70	0.50
68 (non-magnetic)	15	10	5	2	4.3	0.03
68 (0.65 normal magnetic moment)	15	10	5	2	12	0.09

Mean feature diameter 2.1 nm. Compositions in at.%.

showed that precipitates formed with a range of sizes centered at 2.1 nm. The ratio of the scattering perpendicular to the scattering parallel to the magnetic field (A-ratio) was 2.7 slightly lower than observed in BW2. Further analysis (Table 9) using the cluster compositions estimated by FEGSTEM and OPoSAP demonstrated that a consistent solution could be found if it was assumed that the clusters contain iron and have a magnetic moment of 0.65.

4. Summary and discussion

4.1. Microstructural techniques

No single individual technique provided a definitive description of the irradiation-induced copper precipitation in any of the steels analyzed. However, it was shown that, for each steel, the microstructural information from different techniques correlated. In particular in BW2 and CE1, there was good agreement between all three techniques on the size of the copper-enriched precipitates. Furthermore, the FEGSTEM and OPoSAP showed excellent agreement on the level of the bulk copper in the unirradiated material and in the level of matrix copper in the irradiated material. In addition, the composition of the precipitates in both were consistent given that, as detailed in Section 2.2.1.1, it is not possible to measure the level of iron using the FEGSTEM.

The level of iron in the copper-enriched precipitates is still an area of continuing research. Odette and coworkers interpret SANS scattering data as resulting from multi-alloyed precipitates containing little or no iron [20]. However, the OPoSAP data and work reported by Pareige et al. and Miller et al. indicate that appreciable levels of iron exist in the small irradiation-induced precipitates [18,19,21]. This work shows that SANS data can also be interpreted on the basis of copper-enriched precipitates containing appreciable quantities of iron and that this interpretation is consistent with the other microstructural data. Further work is required to fully understand the magnetic properties of these clusters, but a magnetic moment that is lower than the fraction of iron present is consistent with magnetic property measurements performed on pure iron–copper alloys [22].

4.2. Summary of main trends

4.2.1. Low copper base metals

There is little evidence, from the techniques used, for the formation of copper-enriched clusters in either EP2 or EF2 steel (see Table 10). FEGSTEM and OPoSAP microanalysis provided no evidence for significant copper precipitation. SANS detected the presence of a low number density of 1.5 nm diameter features in both EP2 and EF2. Further irradiation of the plate steel led to an increase in number density but no significant change in size. It is not believed that these clusters are contributing strongly to the observed yield strength increase on irradiation. Observations suggest that there is a small increase in phosphorus segregation to the grain boundaries during irradiation. Overall, the results are consistent with the increase in post-irradiation hardness and Charpy properties being due to matrix damage, and this will be discussed in a subsequent paper [23].

4.2.2. High copper weld metals

Table 11 provides a summary of the results from the high copper welds. BW2 and CE1 have the same level of copper in the matrix even though BW2 has a much higher bulk copper content. Following irradiation both BW2 and CE1 have the same level of copper removed from the matrix and precipitated out for the same fluence level. However, there is a greater number density of precipitates in CE1 than in BW2 and they contain somewhat lower copper. The effect of the observed distributions of precipitates on mechanical properties, particularly hardness is discussed in Section 4.3.

Phosphorus increases during irradiation at the grain boundaries for both welds, but the increase is greater in BW2, and the difference is greater than the difference in bulk level suggests.

Table 10
Summary of microstructural data obtained from low copper steels

Irradiation change		EP2 (MTR1)	EP2 (MTR3)	EF2 (MTR1)
Irradiation-induced clustering				
Matrix Cu (wt%)	FEGSTEM	0.10 ± 0.03	0.08 ± 0.03	0.08 ± 0.02
	OPoSAP	0.10 ± 0.01	0.11 ± 0.02	0.07 ± 0.01
Cu precipitated (wt%)	FEGSTEM	<0.01	<0.01	<0.01
	OPoSAP	No evidence of clusters	No evidence of clusters	No evidence of clusters
Cluster diameter (nm)	SANS	1.5	1.4	1.5
Cluster composition	SANS *A*-ratio	1.5	2.3	2.0
Cluster number density (m^{-3})	SANS	$\sim 3 \times 10^{22}$	$\sim 10^{23}$	$\sim 3 \times 10^{22}$
Grain boundary segregation				
P monolayer coverage (%)	FEGSTEM	7	5	4
Mechanical properties				
Hardness	H_v (20 kg load)	196	207	204
Irradiation-induced increase in hardness	H_v (20 kg load)	12	23	14

Table 11
Summary of microstructural data obtained from high copper welds

Irradiation change		BW2 (MTR3)	CE1 (MTR3)
Irradiation-induced clustering			
Matrix Cu (wt%)	FEGSTEM	0.10 ± 0.02	0.10 ± 0.02
	OPoSAP	0.12 ± 0.02	0.13 ± 0.02
Cu precipitated (wt%)	FEGSTEM	0.10 ± 0.03	0.10 ± 0.03
	OPoSAP	0.08 ± 0.03	0.09 ± 0.03
Cluster number density (m^{-3})	OPoSAP	$\sim 1 \times 10^{24}$	$\sim 1 \times 10^{24}$
	SANS	$3–7 \times 10^{23}$	$4–12 \times 10^{23}$
Cluster diameter (nm)	OPoSAP	1.5–2	Insufficient clusters observed to estimate
	SANS	2.1	2.1
Cluster composition (wt%)	FEGSTEM (ignoring Fe)	40 Cu, 24 Ni, 14 Mn, 11 Si, 5 Mo, 4 P	48 Cu, 23 Mn, 21 Ni, 8 Mo
	OPoSAP	~60 Fe, 20–33 Cu, 5–11 Ni, 2–5 Mn, 2–4 Si	~68 Fe, 15 Cu, 10 Mn, 5 Ni, 2 Si
	SANS *A*-ratio	3.1	2.7
Grain boundary segregation			
P monolayer coverage (%)	FEGSTEM	Increased from 6% to 14%	Increased from 2% to 5.5%
Mechanical properties			
Hardness	H_v (20 kg load)	Increased from 208 to 249 VHN	Increased from 193 to 253 VHN
Irradiation-induced increase in hardness	H_v (20 kg load)	41	60

4.2.3. Consistency with mechanisms of irradiation embrittlement

Overall, the irradiation-induced microstructure was consistent with the known mechanisms of RPV embrittlement [1,2]. As expected from the very low bulk levels of copper very little evidence was found for irradiation-induced precipitates in EP2 and EF2. In agreement with other workers [24,25] multi-alloyed copper-enriched clusters were observed in irradiated BW2 and CE1. However, the data summarized in Table 11 demonstrates that there are small differences between the observed microstructures which will

influence the exact level of the contribution to the irradiation-induced hardening from the copper-enriched precipitates (see Section 4.3). The microstructural techniques demonstrated that bulk copper does not necessarily provide a good indication of the potential strengthening increment, $\Delta\sigma_y$, from irradiation-produced precipitation, since copper can be removed from the matrix during post-weld heat-treatment to form large insoluble precipitates on dislocations. Similar effects of heat-treatment on the levels of matrix have been seen by English [26], and Odette et al. [27] in high copper steels.

4.3. Link to mechanical properties

The copper-enriched precipitates/clusters formed during irradiation in the high copper steels can act as barriers to dislocation movement and therefore result in an increase in yield strength and hardness which can be modeled using the Russell–Brown model [7]. The difference between the hardness increment predicted by the Russell–Brown model and the observed hardness increment can be attributed to matrix damage.

Since the microchemical analysis techniques indicated that the precipitates contain not only Cu but also Mn, Ni and Si, and probably Fe, it was necessary to perform a sensitivity analysis to the unknown precipitate modulus. A reference precipitate modulus is 3×10^{10} N/m^2 for a pure bcc copper precipitate. The results showed that the predicted hardness increment from (1) a high number density of precipitates containing iron (high modulus) and (2) a lower number density of precipitates without iron (low modulus) was approximately the same as shown in Table 12 for each weld material. The effect of modulus on computed hardness is shown in Fig. 9.

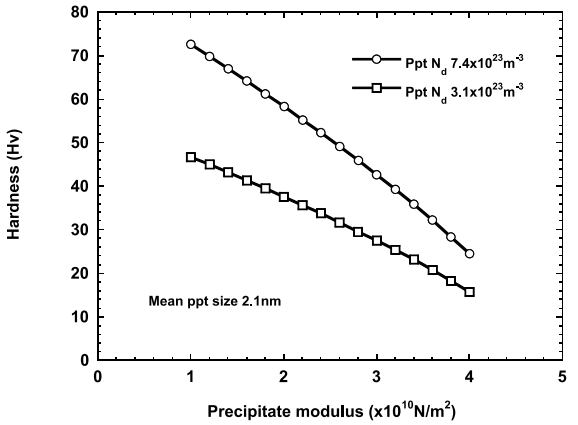

Fig. 9. Effect of precipitate modulus on precipitate hardening (parameters for BW2).

A comparison of the increase in hardness (20 kg) is particularly interesting (see Table 13). For both welds the measured increase in hardness (H_v) is greater than that estimated for the contribution from copper precipitation, providing qualitative support to the methodology adopted for the latter. The difference gives an approximate measure of the contribution from matrix defects. The addition of the various hardening components is non-trivial [28,29]. The two limiting cases, (1) linear sum and (2) the root square sum are summarized in Table 13. The results suggest that the matrix defect contribution to the hardness is smaller in BW2 than CE1.

Table 12
Best estimate of hardening component from Russell–Brown model

Parameter	BW2	BW2	CE1	CE1
Precipitate number density ($\times 10^{23}$ m^{-3})	3.1	7.4	4.3	12
Mean precipitate size (nm)	2.1	2.1	2.1	2.1
Precipitate composition	Cu, Mn, Ni, Si	Fe, Mn, Cu, Ni, Si	Cu, Mn, Ni, Si	Fe, Mn, Cu, Ni, Si
Estimated modulus ($\times 10^{10}$ N/m^2)	2.4	3.4	2.4	3.6
Calculated hardness component (VHN)	34	36	40	41

Table 13
Matrix defect contribution to the hardness in BW2 and CE1

Weld	BW2	CE1
Total hardness change measured on irradiation (VHN) $\Delta H_{v(total)}$	41	60
Estimated hardness contribution from copper precipitates (VHN) (Russell–Brown model) $\Delta H_{v(Cu)}$	~35	~40
Difference assuming linear sum of hardening components $\Delta H_{v(total)} = \Delta H_{v(Cu)} + \Delta H_{v(matrix)}$	~6	~20
Difference assuming root square sum of hardening components $\Delta H_{v(total)}^2 = \Delta H_{v(Cu)}^2 + \Delta H_{v(matrix)}^2$	~23	~45

The difference between total hardness and estimated contribution from precipitation potentially gives a measure of the matrix defect contribution.

5. Conclusions

At present, no microstructural technique has the capability to identify all irradiation-induced microstructural features. However, the combination of FEGSTEM, OPoSAP and SANS provides complementary data on both precipitation and matrix chemistry.

Some segregation of phosphorus to grain boundaries under irradiation was observed in both welds, but there was little measured evidence in either base material.

The results demonstrated that irradiation-induced precipitation is not important in the modern production base materials containing low copper since the irradiation response is dominated by matrix damage. In high copper steels the irradiation response is more complex – both matrix damage and copper-enriched precipitates are generated. The microstructural techniques demonstrated that bulk copper does not necessarily provide a good indication of the potential hardening increment, ΔH_v, from irradiation-produced precipitation, since copper can be removed from the matrix during post-weld heat-treatment to form large insoluble precipitates on dislocations. Furthermore, it was shown that unirradiated matrix chemistry influences the precise precipitate composition, giving rise to copper-enriched precipitates micro-alloyed with Fe, Ni, Mn, and Si. The resulting hardening is strongly influenced by precipitate composition, since this affects the precipitate modulus, and also by the bulk chemistry since this influences precipitate number density.

The Russell–Brown model was used to predict the total change in H_v, due to copper precipitation in the high copper welds, and qualitatively assess the relative importance of copper cluster hardening and matrix damage. The analysis predicted that $\Delta H_{v(Cu)}$ (CE1) is greater than $\Delta H_{v(Cu)}$ (BW2) and, in both cases, less than the total measured hardness. Subtracting the predicted copper contribution from the total measured hardness yields $\Delta H_{v(matrix)}$ (CE1) is greater than $\Delta H_{v(matrix)}$ (BW2). This suggests that matrix damage has a greater effect in CE1 than BW2. These results indicate that embrittlement trends may be distinctly different between different classes of high copper weld.

Acknowledgements

The authors would like to thank Dr Takeo Onchi of CRIEPI for his vision and guidance in the overall direction for this project. The authors would also like to thank Professor R.N. Sinclair of Reading University and Dr M.T. Hutchings of AEAT for their help with the SANS experiments and data interpretation.

References

[1] W.J. Phythian, C.A. English, J. Nucl. Mater. 205 (1993) 162.
[2] G.R. Odette, J. Nucl. Mater. 212–215 (1994) 45.
[3] S. Ishino, T. Kawakami, T. Hidaka, M. Satoh, Nucl. Eng. Des. 119 (1990) 139.
[4] J.T. Buswell, C.A. English, M.G. Hetherington, W.J. Phythian, G.D.W. Smith, G.M. Worrall, in: Effects of Radiation on Materials: 14th International Symposium (volume II), ASTM STP 1046, ASTM, Philadelphia, PA, 1990, p. 127.
[5] A. Cerezo, T.J. Godfrey, S.J. Sijbrandij, G.D.W. Smith, P.J. Warren, Rev. Sci. Instrum. 59 (1998) 862.
[6] G.R. Odette, Mater. Res. Symp. Proc. 373 (1995) 137.
[7] K.C. Russell, L.M. Brown, Acta. Metall. 20 (1972) 969.
[8] S.G. Druce, C.A. English, A.J.E. Foreman, R.J. McElroy, I.A. Vatter, C.J. Bolton, J.T. Buswell, R.J. Jones, in: Effects of Radiation on Materials: 17th International Symposium, ASTM STP 1270, American Society For Testing and Materials, Philadelphia, PA, 1996, p. 119.
[9] Analysis of Capsule OCIII-D: Duke Power Company Oconee Nuclear Station Unit-3, BAW-2128, Rev. 1, May 1992.
[10] Analysis of Capsule OCII-E: Duke Power Company Oconee Nuclear Station Unit-2, BAW-2051, October 1988.
[11] Analysis of Capsule Y: Commonwealth Edison Company Zion Nuclear Plant Unit-1, BAW-2082, March 1990.
[12] Analysis of Capsule Y from the Commonwealth Edison Company Zion Unit-2 Reactor Vessel Radiation Surveillance Program, WCAP-12396, September 1989.
[13] Analysis of Capsule Y from the Pacific Gas and Electric Company Diablo Canyon Unit-1 Reactor Vessel Radiation Surveillance Program, WCAP-13750, July 1993.
[14] D.E. McCabe, et al., in: Heavy Section Steel Irradiation Program Tenth Irradiation Series, ORNL/NRC/LTR-95/18, August 1995.
[15] JEAC 4201, Surveillance Tests of Structural Materials for Nuclear Reactors, Japanese Electric Associations, Japanese Electric Association Codes (JEAC) 4201, 1991.
[16] Regulatory Guide 1.99, Revision 2, Radiation Embrittlement of Reactor Vessel Materials, USNRC, May 1988.
[17] R. McElroy, A.L. Lowe, in: Effects of Radiation on Materials: 17th International Symposium, ASTM 1270, ASTM, Philadelphia, PA, 1996, p. 68.
[18] P. Pareige, R.E. Stoller, K.F. Russel, M.K. Miller, J. Nucl. Mater. 249 (1997) 165.
[19] M.K. Miller, M.G. Burke, in: Effect of Radiation on Materials: 14th International Symposium (volume II), ASTM STP 1046, ASTM, Philadelphia, PA, 1990, p. 107.
[20] G.R. Odette, C.L. Liu, B.D. Wirth, Mater. Res. Symp. Proc. 439 (1997) 457.
[21] P. Pareige, M.K. Miller, Appl. Surf. Sci. 94&95 (1996) 370.
[22] K. Sumiyama, T. Yoshitake, Y. Nakamura, J. Phys. Soc. Jpn. 53 (1984) 3160.
[23] R.G. Carter, N. Soneda, K. Dohi, J.M. Hyde, C.A. English, W. Server, in preparation.
[24] T.J. Williams, W.J. Phythian, in: Effects of Radiation on Materials: 17th International Symposium, ASTM-STP 1270, American Society for Testing and Materials, Philadelphia, PA, 1996, p. 191.

[25] B. Wirth, G.R. Odette, W.A. Pavinich, G.E. Lucas, S.E. Spooner. In: STP 1325, American Society for Testing and Materials, Philadelphia, PA, 1999, p. 102.
[26] C.A. English. In: STP 909, American Society for Testing and Materials, Philadelphia, PA, 1986, p. 187.
[27] G.R. Odette, G.E. Lucas, Radiat. Eff. Defects Solids 189 (1998) 144.
[28] G.R. Odette, MRS Soc. Symp. Proc. 373 (1995) 137.
[29] C.A. English, W.J. Phythian, R.J. McElroy, Mater. Res. Symp. Proc. 439 (1997) 471.